An ^{89}Zr-Labeled PSMA Tracer for PET/CT Imaging of Prostate Cancer Patients

Felix Dietlein[1,2], Carsten Kobe[1], Sergio Muñoz Vázquez[1], Thomas Fischer[1], Heike Endepols[1,3], Melanie Hohberg[1], Manuel Reifegerst[1], Bernd Neumaier[3,4], Klaus Schomäcker*[1], Alexander E. Drzezga*[1,5], and Markus Dietlein*[1]

[1]Department of Nuclear Medicine, University Hospital of Cologne, Cologne, Germany; [2]Department of Medical Oncology, Dana-Farber Cancer Institute, Harvard Medical School, Boston, Massachusetts; [3]Institute of Radiochemistry and Experimental Molecular Imaging, University Hospital of Cologne, Cologne, Germany; [4]Institute of Neuroscience and Medicine, INM-5 (Radiochemistry), Forschungszentrum Jülich GmbH, Jülich, Germany; and [5]Institute of Neuroscience and Medicine, INM-2, Forschungszentrum Jülich GmbH, Jülich, Germany

The short half-life of existing prostate-specific membrane antigen (PSMA) tracers limits their time for internalization into tumor cells after injection, which is an essential prerequisite for robust detection of tumor lesions with low PSMA expression on PET/CT scans. Because of its longer half-life, the ^{89}Zr-labeled ligand ^{89}Zr-PSMA-DFO allows acquisition of PET scans up to 6 d after injection, thereby overcoming the above limitation. We investigated whether ^{89}Zr-PSMA-DFO allowed more sensitive detection of weak PSMA-positive prostate cancer lesions. **Methods:** We selected 14 prostate cancer patients with biochemical recurrence who exhibited no PSMA-positive lesions on a PET scan acquired with existing PSMA tracers (^{68}Ga-PSMA-11, ^{18}F-JK-PSMA-7). Within 5 wk after the negative scan result, we obtained a second PSMA PET scan using ^{89}Zr-PSMA-DFO (117 ± 16 MBq, PET acquisition within 6 d of injection). **Results:** ^{89}Zr-PSMA-DFO detected 15 PSMA-positive lesions in 8 of 14 patients, who had a PET-negative reading of their initial PET scans with existing tracers. In these 8 patients, the new scans revealed localized recurrence of disease (3/8), metastases in lymph nodes (3/8), or lesions at distant sites (2/8). On the basis of these results, patients received lesion-targeted radiotherapies (5/8), androgen deprivation therapies (2/8), or no therapy (1/8). The plausibility of 14 of 15 lesions was supported by histology, clinical follow-up after radiotherapy, or subsequent imaging. Furthermore, comparison of the 15 ^{89}Zr-PSMA-DFO–positive lesions with their correlates on the original PET scan revealed that established tracers exhibited mild accumulation in 7 of 15 lesions; however, contrast-to-noise ratios were too low for robust detection of these lesions (contrast-to-noise ratios, 2.4 ± 3.7 for established tracers vs. 10.2 ± 8.5 for ^{89}Zr-PSMA-DFO, $P = 0.0014$). The SUV_{max} of the 15 ^{89}Zr-PSMA-DFO–positive lesions (11.5 ± 5.8) was significantly higher than the SUV_{max} on the original PET scans (4.7 ± 2.8, $P = 0.0001$). Kidneys were the most exposed organ, with doses of 3.3 ± 0.7 mGy/MBq. The effective dose was 0.15 ± 0.04 mSv/MBq. **Conclusion:** In patients with weak PSMA expression, a longer period of time might be needed for ligand internalization than that offered by existing PSMA tracers to make lesions visible on PET/CT scans. Hence, ^{89}Zr-PSMA-DFO might be of significant benefit to patients in whom the search for weak PSMA-positive lesions is challenging. Radiation exposure should be weighed against the potential benefit of metastasis-directed therapy or salvage radiotherapy, which we initiated in 36% (5/14) of our patients based on their ^{89}Zr-PSMA-DFO PET scans.

Key Words: prostate cancer; PET; PSMA tracer; ^{89}Zr-PSMA-DFO; ^{68}Ga-PSMA-11; ^{18}F-JK-PSMA-7

J Nucl Med 2022; 63:573–583
DOI: 10.2967/jnumed.121.262290

In a substantial number of prostate cancer patients, prostate-specific antigen (PSA) serum levels rise after surgery or radiotherapy (biochemical recurrence [BCR]). Early localization of recurrent tumor lesions is critical for selecting the accurate salvage therapy to improve the survival of these patients. Prostate-specific membrane antigen (PSMA) PET/CT imaging is widely used for localizing prostate cancer after BCR, and an extensive series of clinical studies has established the increased detection rate of PSMA tracers relative to alternative PET tracers or imaging techniques (*1,2*). Nevertheless, PSMA PET scans fail to localize tumor lesions in approximately 20% of the patients with BCR (*3*). In a series of prostatectomies, PSMA staining intensity was reported as absent or weak for 23% and 19% of patients with malignant tissue and Gleason scores of 3 + 4 or 4 + 3, respectively (*4*). Furthermore, negative PSMA PET scan results are significantly associated with weak PSMA levels based on immunohistochemistry (*5*). This might explain why PSMA PET scans reveal negative results in a substantial number of prostate cancer patients, even at high PSA levels. Patients with detectable but weak PSMA expression in the recurrent tumor lesions pose a challenge for existing PSMA ligands.

One limitation of existing PSMA tracers is the short half-life of their radioactive labels (^{18}F: 1.8 h, ^{68}Ga: 1.1 h), which means that PET images must be acquired within 3 h of injection. Experimental data suggest, however, that internalization of PSMA ligands gradually increases over 24 h (*6*). Ligand internalization is an important prerequisite for tracer accumulation in recurrent tumor lesions. Moreover, mildly increased tumor-to-background ratios could be observed with existing tracers when PET/CT scans were acquired later (3 h vs. 1 h) after tracer injection (*7,8*). Hence, if PET/CT images could be acquired much later, such as days after injection, even prostate cancer lesions with weak PSMA expression might become detectable on PSMA PET scans.

Given that existing PSMA tracers cannot overcome this limitation due to their short half-lives, we explored the value of a new

Received Mar. 11, 2021; revision accepted Jun. 29, 2021.
For correspondence or reprints, contact Markus Dietlein (markus.dietlein@uk-koeln.de).
*Contributed equally to this work.
Published online Jul. 29, 2021.

^{89}Zr-labeled PSMA tracer (^{89}Zr-PSMA-DFO) in prostate patients with BCR. Unlike existing PSMA tracers, the long half-life of the ^{89}Zr label (77 h) allows image acquisition several days after tracer injection. Furthermore, our ex vivo data on LNCaP tumor xenograft–bearing mice revealed that ^{89}Zr-PSMA-DFO exhibited an increased tumor-to-background ratio compared with the widely used PSMA tracers ^{68}Ga-PSMA-11 and ^{18}F-JK-PSMA-7 due to a prolonged period for ligand internalization (*6*). Moreover, many existing PSMA tracers are excreted through the kidney, and ^{89}Zr-PSMA-DFO might improve the detection of tumor lesions in lymph nodes near the ureter after renal clearance. Here, we present the first-in-humans application of ^{89}Zr-PSMA-DFO for PET imaging in 14 prostate cancer patients after BCR. Using ^{89}Zr-PSMA-DFO, we aimed to identify tumor lesions for metastasis-directed therapy (MTD) or salvage radiotherapy (S-RT) in these 14 patients, who had negative PET scan results using existing PSMA tracers (^{68}Ga-PSMA-11, ^{18}F-JK-PSMA-7). We also compared ^{89}Zr-PSMA-DFO–positive lesions with their correlates in the initial, negative PET scan results and examined the clinical plausibility of the ^{89}Zr-PSMA-DFO–positive lesions.

MATERIALS AND METHODS

Patient Characteristics

Patients with biochemically relapsed prostate cancer underwent PET/CT imaging with the widely used tracers ^{68}Ga-PSMA-11 or ^{18}F-JK-PSMA-7 as part of clinical routine diagnostics. The first PET scan was read as entirely PSMA-negative (13/14) or exhibited PSMA-positive findings exclusively in or near the urinary tract, which were interpreted as residual activity in the urine (1/14). When the irradiation of an empiric field within the prostate fossa was no longer an option, since either S-RT had already been performed after prostatectomy (11/14), or S-RT after prostatectomy had been refused by the patient before imaging (2/14), or radiotherapy had already been performed as the first-line therapy (1/14), we offered a second PET scan with ^{89}Zr-PSMA-DFO. Between December 2019 and July 2020, 14 patients were interested in a second PET scan because these patients were in good condition and expressed a clear preference for a MTD over an androgen deprivation therapy (ADT). The 14 patients were selected from an overall group of 633 patients, who underwent PSMA PET/CT within the 8 mo of recruitment.

In these 14 patients (average age, 62.1 ± 8.6 y), we performed a second PET scan using ^{89}Zr-PSMA-DFO within 5 wk of the first scan. Most patients (11/14) had undergone 2 therapy lines for prostate cancer (i.e., prostatectomy followed by S-RT with an empiric field). Two patients had undergone only initial prostatectomy, and 1 patient had received radiotherapy alone. Tables 1 and 2 provide more details on patient characteristics. Because the option of MDT or S-RT depends on the exact localization of the tumor and no other PSMA tracers or imaging options with comparable sensitivity are available, we determined that the benefit of the PET imaging outweighed the radiation exposure of an additional PET/CT scan using the ^{89}Zr-labeled ligand. The Institutional Review Board approved this study and the use of the data for a retrospective analysis. All subjects signed a written informed consent form to PET imaging and the use of their data for a retrospective analysis. All procedures were performed in compliance with the regulations of the responsible local authorities (District Administration of Cologne, Germany).

Tracer Preparation

^{89}Zr-PSMA-DFO was produced following applicable good manufacturing practice (*6*). The precursor for the ^{89}Zr-based PSMA-vector EuK-2NaI-AMCHA-N-sucDf-Fe (E = glutamic acid, u = urea, K = lysine, 2Nal = 2-naphthyl-alanine, AMCHA = traxamic acid) (ABX) was formed by the pharmacophore EuK coupled to a naphthylic linker and the chelator agent N-sucDf-Fe. The N-sucDf-Fe moiety functionalized the molecule for labeling with ^{89}Zr. It proved to be a suitable chelator for ^{89}Zr. Labeling of the precursor Fe-N-PSMA-Df with ^{89}Zr required a multistep procedure due to the presence of Fe(III), which was removed by transchelation to ethylenediaminetetraacetic acid (EDTA) (100:1) at 35°C for 30 min, forming [Fe(III)EDTA]. The purification of the Fe(III)-free compound from byproducts such as EDTA and [Fe(III)EDTA] was performed using a Sep-Pak C_{18} plus light cartridge (130 mg of sorbent per cartridge, 55- to 105-μm particle size) (Waters Corp.) and PD MidiTrap G-10 column (>700 Mr, 5.3-mL bed package of Sephadex G-10) (GE Healthcare). After elution of PSMA-Df, the radiolabeling procedure was performed by adjusting the pH of a solution of ^{89}Zr in 1 M oxalic acid to 6.8–7.2 with 1 M sodium carbonate, 0.5 M *N*-(2-hydroxyethyl)piperazine-*N*′-(2-ethanesulfonic acid) (HEPES) (pH 6.8), and 0.25 M sodium acetate (5 mg/1 mL gentisic acid, 50 μL). Unbound ^{89}Zr was then efficiently removed by solid-phase extraction using a Sep-Pak C_{18} plus light cartridge.

Specification of ^{89}Zr-PSMA-DFO and quality control included assessment of radiochemical purity (≥97%), pH-value (5.0–8.0), endotoxin content (≤11.7 IE/mL), testing for sterility, and chemical purity (HEPES ≤ 40 μg/mL, ethanol ≤ 10%). During this study, none of the 7 syntheses failed to reach these specifications.

Imaging and Reading

All PET/CT images were acquired from midthigh to the tip of the skull on a Biograph mCT 128 Flow PET/CT scanner (Siemens Healthineers) and reconstructed using an ultra-high-definition (UHD) algorithm. For existing PSMA tracers, PET scans were acquired 1 h (^{68}Ga-PSMA-11, 153 ± 30 MBq, 4 patients) or 2 h (^{18}F-JK-PSMA-7, 286 ± 26 MBq, 10 patients) after injection. For ^{89}Zr-PSMA-DFO (117 ± 16 MBq), we acquired PET/CT scans 2 and 3 d after tracer injection (10 patients). For logistical reasons, we slightly deviated from this protocol for 4 patients (images acquired on days 1 and 2, or on days 1 and 3, or on days 2 and 6, or on days 1, 2, and 6, respectively). Acquisition times were adapted to the PSMA ligand with a flow motion bed speed of 1.5 mm/s for ^{68}Ga-PSMA-11 and ^{18}F-JK-PSMA-7, of 0.9 mm/s for the first ^{89}Zr-PSMA-DFO PET scan, and of 0.6 mm/s for the subsequent ^{89}Zr-PSMA-DFO PET scans. CT scans (slice thickness of 5.0 mm, pitch 1.2) were acquired using a low-dose technique with kV and mA modulation adapted to the patient's size.

Because we applied lower activities of ^{89}Zr-PSMA-DFO than of ^{68}Ga-PSMA-11 or ^{18}F-JK-PSMA-7, we measured the signal-to-noise ratio (SNR) and the contrast-to-noise ratio (CNR) to describe the image quality obtained with ^{89}Zr-PSMA-DFO on the Biograph mCT 128 Flow PET/CT scanner (*9*). The SNR was calculated as the ratio of SUV_{mean} to SD in a volume of interest (VOI) with 3-cm diameter in the liver. The CNR was calculated as the ratio of the difference of the SUV_{mean} in the lesion and the SUV_{mean} in the background to SD in the background. The SUV_{mean} in a lesion was obtained by delineating a VOI at 41% of the SUV_{max} of the same lesion. The SUV_{mean} of the background and its SD were measured in a 3-cm VOI in the local background around the lesion.

For cross-calibration of the ^{89}Zr label, we filled an ^{89}Zr-phantom with 6.283 L of a specific activity of ^{89}Zr (43.287 MBq/L). The activity of ^{89}Zr, measured by the PET/CT scanner, was 35.597 MBq/L, resulting in a dose cross-calibration factor of 1.216. To avoid overestimating the SUV in ^{89}Zr-PSMA-DFO–positive tumor lesions with the UHD algorithm (*10*), we did not multiply ^{89}Zr-PSMA-DFO SUVs by the cross-calibration factor for ^{89}Zr. The cross-calibration factors for ^{68}Ga and ^{18}F were 1.01 and 1.02, respectively.

PET/CT scans were interpreted according to published criteria for standardization of PSMA PET/CT interpretation (*11,12*) by a team of 2 specialists in nuclear medicine and 1 radiologist. Any disagreement

was resolved in consensus. The same team interpreted PET/CT scans acquired with ^{89}Zr-PSMA-DFO and existing PSMA tracers (^{68}Ga-PSMA-11, ^{18}F-JK-PSMA-7). Statistical analyses were performed with Microsoft Excel, comparing the SUVs in the areas with a suspicious PSMA accumulation, the SNRs, and the CNRs.

Dosimetric Measurement

Estimation of the kidney dose was determined on the basis of 3 patients who underwent PET/CT scans with an interval between 2 scans of at least 2 d. The following assumptions were made for the estimation: between time 0 (injection) and the first measuring point the time–activity curve has a constant progression. All measuring points were integrated numerically using trapezoidal approximation. From the last measuring point to infinity, a monoexponential function was fitted and integrated. As the effective half-life could not be accurately determined from 2 measurement points in 2 of the 3 patients, the physical half-life of ^{89}Zr was used instead.

RESULTS

PSMA-Positive Lesions with ^{89}Zr-PSMA-DFO PET

We acquired ^{89}Zr-PSMA-DFO PET/CT scans of 14 patients with BCR, who had been examined with ^{68}Ga-PSMA-11 ($n = 4$) or ^{18}F-JK-PSMA-7 ($n = 10$) less than 5 wk previously without any PSMA-positive tumor lesions being revealed (Tables 1 and 2). In 8 of 14 patients (57%), ^{89}Zr-PSMA-DFO identified at least 1 PSMA-positive lesion (15 additional lesions in total). We detected these lesions in the prostate or prostate fossa of 3 patients, in lymph nodes of 3 patients, and at distant lesions for 2 patients (bone marrow, lung). In addition, we interpreted PSMA-positive lesions according to PSMA-RADS version 1.0 and the miTNM classification (Tables 1 and 2). To avoid false-positive interpretations because of low SNRs, we applied the following additional criteria: we interpreted a lesion as PSMA-positive, if it could be detected on 2 independent scans (14/15 lesions); and we interpreted a PSMA-positive lesion as a PSMA-positive lymph node or as a suspicious lung lesion, if we detected a radiologic correlate on the parallel low-dose CT scan.

To examine which aspects might have contributed to the detection of these 15 additional lesions, we compared lesions identified by ^{89}Zr-PSMA-DFO with the corresponding areas on the initial PET scans (^{68}Ga-PSMA-11, ^{18}F-JK-PSMA-7), using the mediastinal blood pool as a reference. This comparison revealed that 7 of 15 lesions also exhibited a mild tracer accumulation on the PET scans acquired with ^{68}Ga-PSMA-11 or ^{18}F-JK-PSMA-7 (average ratio of the tumor area to the mediastinal blood pool for both tracers: 3.1 ± 2.4; ^{68}Ga-PSMA-11: 2.6 ± 1.8; ^{18}F-JK-PSMA-7: 3.5 ± 2.9), but that this signal was not strong enough to allow robust detection of those lesions.

In contrast, PET/CT scans acquired with ^{89}Zr-PSMA-DFO exhibited a significantly higher ratio of the 15 lesions to the mediastinal blood pool (14.2 ± 7.7, $P < 0.0001$, paired t test), and this difference remained significant when comparing the signal of ^{89}Zr-PSMA-DFO with that of ^{68}Ga-PSMA-11 ($P = 0.0072$, 7 lesions, Figs. 1 and 2) and ^{18}F-JK-PSMA-7 ($P = 0.026$, 8 lesions, Fig. 3) separately (Tables 3 and 4). When we used the SUV_{max} as an alternative measure, these differences were similarly significant ($P = 0.0002$), and the corresponding numbers were 4.7 ± 2.0 (^{68}Ga-PSMA-11), 4.7 ± 3.5 (^{18}F-JK-PSMA-7), and 11.1 ± 5.8 (^{89}Zr-PSMA-DFO).

Furthermore, like many existing PSMA tracers, ^{68}Ga-PSMA-11 and ^{18}F-JK-PSMA-7 are excreted through the kidney, which interferes with the detection of lesions near the ureter due to residual activity in the urine. The ^{89}Zr-PSMA-DFO PET scans were uncompromised by residual activity in the urinary tract, because they were acquired after the tracer was fully cleared from the bloodstream. This might have facilitated the detection of tumor lesions near the ureter (Supplemental Fig. 1).

Image Quality

SNRs of ^{89}Zr-PSMA-DFO were 2.1 ± 0.5 and 2.1 ± 0.4 in the first and second PET scans, respectively. These ratios were significantly lower than those of established tracers (SNR of ^{68}Ga-PSMA-11: 3.7 ± 0.9, $P = 0.0034$; SNR of ^{18}F-JK-PSMA-7: 7.7 ± 1.3, $P < 0.0001$, paired t test) (Table 5). However, ^{89}Zr-PSMA-DFO PET/CT exhibited significantly higher CNRs in PSMA-positive lesions (10.2 ± 8.5 and 11.0 ± 10.1 in scans 1 and 2) than ^{68}Ga-PSMA-11 (4.5 ± 4.6, $P = 0.0016$), ^{18}F-JK-PSMA-7 (0.7 ± 1.0, $P = 0.036$), or ^{68}Ga- and ^{18}F-PSMA tracers in combination (2.4 ± 3.7, $P = 0.0014$, paired t test) (Table 6, Supplemental Table 1). This suggests that the detection of weak PSMA-avid lesions was facilitated by significantly higher CNR of ^{89}Zr-PSMA-DFO.

Timing Between Tracer Injection and ^{89}Zr-PSMA-DFO PET Scans

Finally, we investigated whether the time between injection and image acquisition had a substantial impact on the sensitivity of ^{89}Zr-PSMA-DFO. For all tumor patients, we acquired PET/CT scans with ^{89}Zr-PSMA-DFO on 2 or more days after tracer injection (2 whole-body scans for 13 patients, 3 whole-body scans for 1 patient). Most lesions (14/15) were visible on all consecutive scans. Only 1 lesion became visible on day 6 only (SUV_{max} 8.1) and could not be detected previously (day 1: SUV_{max} 3.2; day 2: SUV_{max} 2.5). The SNR did not differ significantly between first (2.1 ± 0.5) and second (2.1 ± 0.4) ^{89}Zr-PSMA-DFO PET scans ($P = 0.79$, paired t test). CNRs of the 15 PSMA-positive lesions did not differ significantly between scans 1 and 2 either (10.2 ± 8.5 vs. 11.0 ± 10.1, $P = 0.69$, paired t test). Similar results were obtained when using the SUV_{max} instead (11.5 ± 5.8 vs. 9.9 ± 5.1, $P = 0.27$) (Tables 3 and 6), suggesting that the exact time of acquisition has no more than a minor impact on detection of PSMA lesions, as long as PET/CT images are acquired at least 2 d after tracer injection when ligand internalization has reached a steady state.

Verification and Therapeutic Consequences

We verified ^{89}Zr-PSMA-DFO–positive lesions in 5 of 8 patients by histology (1 patient) and clinical follow-up (4 patients, drop-in PSA levels after metastasis-directed radiotherapy). On the basis of the results of the ^{89}Zr-PSMA-DFO PET/CT scan, these 5 patients received MDT or S-RT (3 patients: prostate fossa, 1 patient: PSMA-positive lymph-nodes, 1 patient: solitary bone marrow metastasis). Another 2 patients with ^{89}Zr-PSMA-DFO–positive PET scan results received ADT because they were not eligible for MDT. One patient with a PSMA-positive coin lesion in the lung exhibited stable disease in a follow-up CT after 7 mo and PSA levels remained stable for 11 mo, so that the urologists pursued watchful waiting for this patient. Further data on clinical follow-up are presented in Tables 1 and 2.

Dosimetric Measurement

The ^{89}Zr-PSMA-DFO PET scans exhibited the highest tracer activity in the kidneys, the organ with the highest radiation exposure. We calculated the kidney dose to be 3.3 ± 0.73 mGy/MBq. The overall effective dose (*13*) was 0.15 ± 0.04 mSv/MBq.

TABLE 1
Clinical Data from Patients 1–7 with PET-1 Scan Results Interpreted as PSMA-Negative

Patient	Indication	Gleason score, TNM	PSA value, dt PSA, and iPSA	PSMA tracer used in PET-1	No. of lesions interpreted as PSMA-positive with ^{89}Zr-PSMA-DFO in PET-2	Therapeutic consequence	Verification
1	BCR after RT	NA, NA	3.2, >12 mo, 4.21	^{18}F-JK-PSMA-7	Prostate lobe right PSMA-RADS 4 Prostate lobe left PSMA-RADS 4 miT2mN0M0	Biopsy, S-RT at a PSA level of 4.2	Histologically confirmed on both sides. Decrease in PSA level to 1.5 after S-RT
2	BCR after RPE and S-RT	4 + 3, pT2 cN0	0.88, >12 mo, 4.53	^{68}Ga-PSMA-11	Coin lesion in the lung, dignity unclear PSMA-RADS 3C miT0N0M1c	Watchful waiting with low-dose CT of the lung	Stable in the CT of the lung after 7 mo, PSA stable after 11 mo, suggestive of vascular malformation
3	BCR after RPE and S-RT	3 + 4, pT3a pN0	7.2, 4 mo, 12	^{18}F-JK-PSMA-7	3 l.n. retroperitoneal PSMA-RADS 3A l.n. supraclav. left PSMA-RADS 3A miT0N1bM0	ADT after rapid increase of PSA to 14.6	Increase in PSA level before ADT
4	BCR after RT and S-RPE	4 + 5, Tx pN1	0.46, 3 mo, NA	^{18}F-JK-PSMA-7	None PSMA-RADS 0 miT0N0M0	Watchful waiting with PSMA PET/CT	PSMA-negative, bone metastases detected after 9 mo
5	BCR after RPE. ADT until 12 mo before	5 + 5, pT4 pN0	0.31, NA, 444	^{18}F-JK-PSMA-7	None PSMA-RADS 0 miT0N0M0	Start with ADT at a PSA level of 1.74. S-RT of the prostate fossa	Decrease in PSA level to 0.03 after S-RT and ADT
6	BCR after RPE and S-RT	4 + 4, pT2a pN0	0.72, 7 mo, 13.15	^{68}Ga-PSMA-11	l.n. iliac right PSMA-RADS 3A Os ilium left PSMA-RADS 3B miT0N1aM1b	RT of the solitary bone metastasis at a PSA level of >1, RT of the l.n. iliac right 9 mo later	Decrease in PSA level to 0.71 after RT; ^{18}F-JK-PSMA PET/CT after 9 mo: progress of the l.n. iliac right
7	BCR after RPE and S-RT	3 + 4, pT3b pN0	0.62, 3 mo, 7.1	^{18}F-JK-PSMA-7	None PSMA-RADS 0 miT0N0M0	Watchful waiting with PSMA PET/CT	PET/CT after 6 mo also PSMA-negative at a PSA level of 1.3

TABLE 2
Clinical Data from Patients 8–14 with PET-1 Scan Results Interpreted as PSMA-Negative

Patient	Indication	Gleason score, TNM	PSA value, dt PSA, and iPSA	PSMA tracer used in PET-1	No. of lesions interpreted as PSMA-positive with ^{89}Zr-PSMA-DFO in PET-2	Therapeutic consequence	Verification
8	BCR after RPE and S-RT	3 + 4, pT2 pN1	4.4, 5 mo, 24	^{68}Ga-PSMA-11	2 l.n. retroperitoneal PSMA-RADS 3A l.n. supraclav. left PSMA-RADS 3A miT0N1bM0	All 3 PSMA-positive l.n. treated with S-RT; start of temporary ADT	Decrease in PSA level to 0.17 ng/mL
9	BCR after RPE and S-RT	4 + 3, pT3 pN0	1.1, >12 mo, 14	^{18}F-JK-PSMA-7	None PSMA-RADS 0 miT0N0M0	Watchful waiting	MRI also without finding
10	BCR after RPE. S-RT refused before PET	4 + 4, pT3a pN0	0.54, 10 mo, 7.7	^{18}F-JK-PSMA-7	Prostate fossa right PSMA-RADS 4 miT2uN0M0	S-RT	Decrease in PSA level to 0.3 after S-RT
11	BCR after RPE and S-RT. ADT until 2 y before	4 + 5, pT3b pN0 R1	0.81, NA, 184	^{18}F-JK-PSMA-7	None PSMA-RADS 0 miT0N0M0	Start with ADT at a PSA level of 1.71	MRI also without finding
12	BCR after RPE and S-RT	3 + 4, NA	1.78, 4 mo, 6.2	^{18}F-JK-PSMA-7	None PSMA-RADS 0 miT0N0M0	Start with ADT for 1 y	MRI also without finding
13	BCR after RPE and S-RT	4 + 3, pT3b pN0	2.01, 1 mo, 8.5	^{68}Ga-PSMA-11	l.n. iliac right PSMA-RADS 3A miT0N1aM0	Start with ADT at a PSA level of 3.8	MRI with enlarged l.n. iliac right
14	BCR after RPE. S-RT not recommended before PET	3 + 4, pT2c pN0	0.7, 7 mo, NA	^{18}F-JK-PSMA-7	Prostate fossa left PSMA-RADS 4 miT2uN0M0	S-RT	Decrease in PSA level to 0.09 after S-RT (6 wk after the end of S-RT)

Eight of the 14 patients showed PSMA-positive lesions with ^{89}Zr-PSMA-DFO. In 6 patients, the PSMA-negative interpretation from PET-1 was confirmed by the ^{89}Zr-PSMA-DFO PET-2. The location of each PSMA-positive lesion detected with ^{89}Zr-PSMA-DFO is described for each patient.

dtPSA = doubling time of PSA; iPSA = initial PSA; l.n. = lymph node; NA = not available; RPE = radical prostatectomy; RT = radiotherapy.

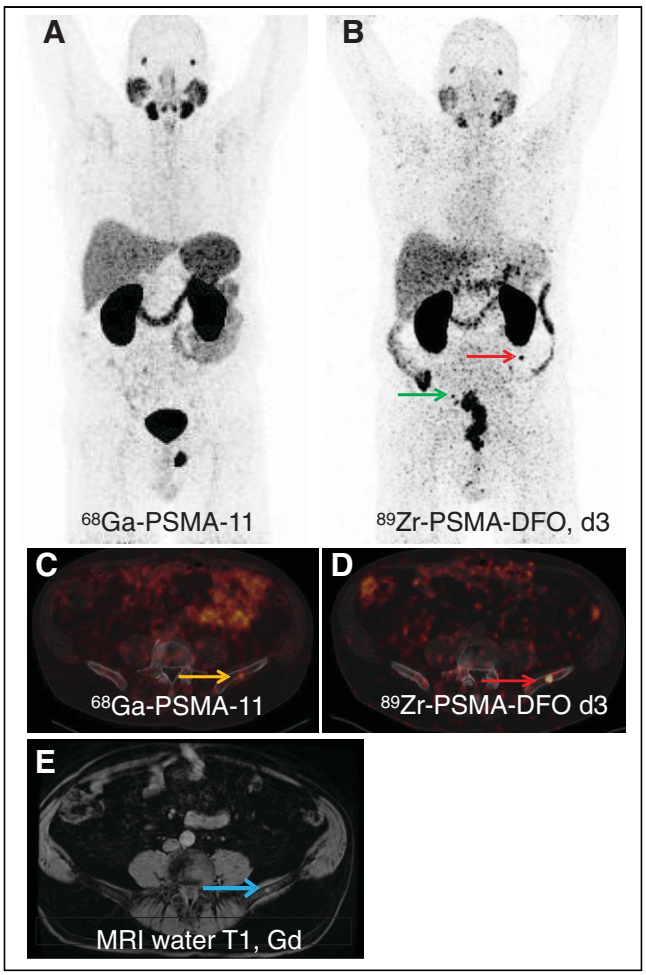

FIGURE 1. ^{68}Ga-PSMA-11 PET with maximum-intensity-projection (MIP) (A) and PET/low-dose CT fusion images (C), and ^{89}Zr-PSMA-DFO PET 3 d after injection with MIP (B) and PET/low-dose CT fusion images (D) of patient 6 with BCR after prostatectomy and S-RT. Images are highly suggestive of a PSMA-positive osteomedullary metastasis in os ilium left, clearly visible with ^{89}Zr-PSMA-DFO (red arrows in B and D). PSMA overexpression in os ilium left with ^{68}Ga-PSMA-11 was faint (yellow arrow in C). Small lesion is retrospectively visible in the MRI scan (blue arrow in E) without any correlate in low-dose CT. After PSA level further increased above 1 ng/mL, bone metastasis was irradiated and PSA levels dropped to 0.7 ng/mL. Nine months later, ^{18}F-JK-PSMA-7 PET/CT revealed further progression of tumor in right iliac lymph node with weak ^{89}Zr-PSMA-DFO expression (green arrow in B), and the lymph node was locally irradiated. d = day; Gd = gadolinium; p.i. = after injection.

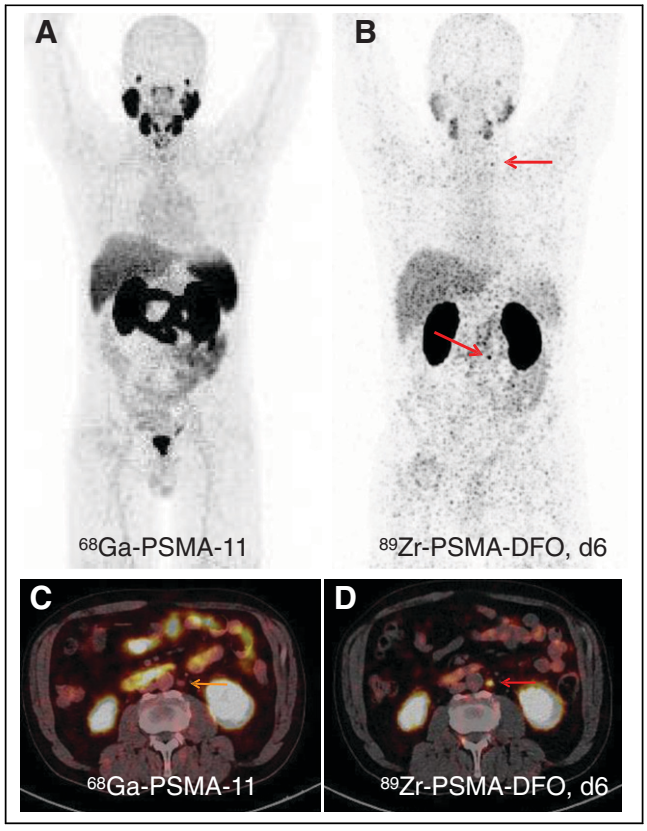

FIGURE 2. ^{68}Ga-PSMA-11 PET with maximum-intensity-projection (MIP) (A) and PET/low-dose CT fusion images (C), and ^{89}Zr-PSMA-DFO PET 6 d after injection with MIP (B) and PET/low-dose CT fusion images (D) of patient 8 with BCR after prostatectomy and S-RT. Images are highly suggestive of PSMA-positive lymph node metastases supraclavicular left and retroperitoneal left, visible with ^{89}Zr-PSMA-DFO (red arrows in B and D). Lymph nodes were PSMA-negative with ^{68}Ga-PSMA-11 (yellow arrow in C). Patient underwent S-RT and temporary ADT. PSA level dropped to 0.17 ng/mL. d = day; p.i. = after injection.

Adverse Events

All patients tolerated the tracer injection and the PET/CT examination well. We asked each patient whether they had experienced any adverse side effects when the PET results were communicated with the patient in person and again when the therapeutic consequences were discussed on the phone. None of the patients reported nausea, diarrhea, dizziness, or any other adverse events or side effects during these conversations.

DISCUSSION

Our study revealed that ^{89}Zr-PSMA-DFO has the ability to localize lesions with weak PSMA expression in patients with BCR when the preceding ^{68}Ga-PSMA-11 or ^{18}F-JK-PSMA-7 PET scans have been read as PSMA-negative. In our small group, localization was successful in more than half of the prostate cancer patients (8/14). This observation is in marked contrast to the results obtained with other PSMA tracers we have examined recently. For example, when comparing ^{68}Ga-PSMA-11 with ^{18}F-DCFPyL, we obtained an ^{18}F-DCFPyL–positive PET scan after a prior ^{68}Ga-PSMA-11–negative scan in only 1 of 25 patients (*3,14*). Similarly, ^{18}F-JK-PSMA-7 (1/10 patients) and ^{18}F-PSMA-1007 (0/7 patients) rarely revealed a positive scan result after a previous negative PET scan result (*15,16*). Hence, our study demonstrates that ^{89}Zr-PSMA-DFO has the ability to identify tumor lesions with detectable but low PSMA expression.

In this study, ^{89}Zr-PSMA-DFO PET was offered with the goal of initiating MDT and delaying the start of ADT with the risk of later castration resistance. MDT is described as a promising therapeutic approach in men with hormone-sensitive oligometastatic prostate cancer with up to 3 metastases in international guidelines, but its efficacy depends on the exact and sensitive localization of all tumor lesions (*17,18*). In a phase 2 randomized study, MDT of the PSMA-positive lesions improved the progression-free survival and decreased the risk of new lesions in the PSMA PET at 6 mo (*19*). On the basis of the ^{89}Zr-PSMA-DFO PET scans, an MDT or S-RT could be initiated in 5 of 14 patients. However, this clinical

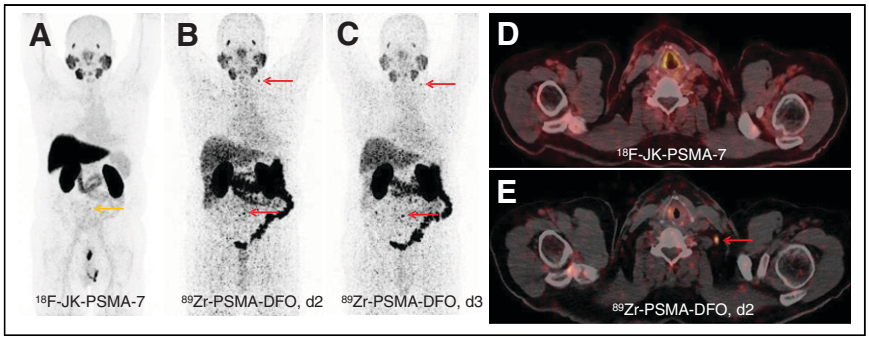

FIGURE 3. ^{18}F-JK-PSMA-7 PET with maximum-intensity-projection (MIP) (A) and PET/low-dose CT fusion images (D), and ^{89}Zr-PSMA-DFO PET 2 and 3 d after injection with MIP (B and C) and PET/low-dose CT fusion images (E) of patient 3 with BCR after prostatectomy and S-RT. Images are highly suggestive of PSMA-positive lymph node metastases supraclavicular left and retroperitoneal, visible with ^{89}Zr-PSMA-DFO (red arrows in B, C, and E). Lymph node supraclavicular left was PSMA-negative with ^{18}F-JK-PSMA-7, and lymph node retroperitoneal was faintly PSMA-positive with ^{18}F-JK-PSMA-7 (yellow arrow in A). Because of rapid increase in PSA level, patient underwent ADT. D = day; p.i. = after injection.

benefit required an ^{89}Zr-PSMA-DFO PET/CT scan, resulting in a radiation exposure of 3.3 ± 0.73 mGy/MBq for the kidneys and an overall effective dose of 0.15 ± 0.04 mSv/MBq. Our dosimetry estimates suggest that the effective dose of ^{89}Zr-PSMA-DFO is lower than that of an ^{89}Zr-labeled antibody in metastatic castration-resistant prostate cancer patients (0.44 mSv/MBq), but the renal dose of ^{89}Zr-PSMA-DFO is higher than that of an ^{89}Zr-labeled antibody (0.73 mSv/MBq) (*20*). Dosimetry estimates in larger patient cohorts will be required to establish ^{89}Zr-PSMA-DFO in routine clinical diagnostics.

Multiple orthogonal observations suggest that the prolonged acquisition time after tracer injection led to increased accumulation of ^{89}Zr-PSMA-DFO in prostate cancer lesions. First, comparison of matched PET scans revealed that ^{68}Ga-PSMA-11 and ^{18}F-JK-PSMA-7 also accumulated in the lesions identified by ^{89}Zr-PSMA-DFO, suggesting that the 3 ligands consistently bound to the surface of these tumor cells. However, prolonged time was required for sufficient ligand internalization, so that these lesions could be identified only on ^{89}Zr-PSMA-DFO PET/CT scans. Second, experimental studies suggest that internalization of PSMA ligands increases over time, thereby gradually enhancing the signal-to-background ratio (*6*). Third, recent clinical studies have indicated that the performance of existing tracers can be marginally improved by acquiring PET images with ^{68}Ga-PSMA-11 or ^{18}F-JK-PSMA-7 at later time points (*7,8*). Fourth, many tracers are excreted through the kidney, and acquisition at later time points facilitates detection of lesions near the ureter due to low residual activity in the urine. As such, ^{89}Zr-PSMA-DFO might be particularly suitable for detecting tumor lesions with low PSMA expression.

Our study further suggests that images with ^{89}Zr-PSMA-DFO can be acquired anytime 48–72 h after tracer injection. The exact acquisition time point within this period has only a marginal impact on tracer sensitivity (half-life of ^{89}Zr-PSMA-DFO is 77 h).

TABLE 3
SUV_{max} Values from 8 Patients with PET-2 Scan Results Interpreted as PSMA-Positive with ^{89}Zr-PSMA-DFO

	Lesions interpreted as PSMA-positive with ^{89}Zr-PSMA-DFO in PET-2						
Patient	PET finding	SUV_{max}, day 1	SUV_{max}, day 2	SUV_{max}, day 3	SUV_{max}, day 6	Corresponding area with ^{18}F-JK-PSMA-7 in PET-1, SUV_{max} (2 h)	Corresponding area with ^{68}Ga-PSMA-11 in PET-1, SUV_{max} (1 h)
1	Prostate lobe right		13.3	13.1		5.4	
	Prostate lobe left		9.5	7.1		4.6	
2	Lung left (dignity unclear)		5.7		6.7		4.1
3	l.n. retroperitoneal		3.1	6.1		1.4	
	l.n. retroperitoneal		17.0	11.0		2.4	
	l.n. retroperitoneal		14.2	8.9		1.7	
	l.n. supraclav. left		12.1	6.9		2.2	
6	l.n. iliac right		7.8	13.2			4.3
	Os ilium left		14.3	15.8			8.2
8	l.n. retroperitoneal	11.5	9.6		15.6		3.1
	l.n. retroperitoneal	12.2	8.3		7.2		6.0
	l.n. supraclav. left	3.2	2.5		8.1		2.0
10	Prostate fossa right		14.7	22.8	11.1	10.9	
13	l.n. iliac right		7.6	4.5			5.5
14	Prostate fossa left		25.5	12.8		8.7	

When one or several PSMA-positive areas were detected by ^{89}Zr-PSMA-DFO PET, the SUV_{max} within the corresponding area of the ^{18}F-JK-PSMA-7 or the ^{68}Ga-PSMA-11 PET scan was measured. The SUV_{max} of ^{89}Zr-PSMA-DFO PET-2 (first measurement) was significantly higher than the SUV_{max} of the PET-1 scan with ^{68}Ga-PSMA-11 or ^{18}F-JK-PSMA-7 in the corresponding areas ($P = 0.0001$, paired t test).

l.n. = lymph node.

TABLE 4
SUV Ratios from 8 Patients Whose PET-2 scans Were Interpreted as PSMA-Positive with ^{89}Zr-PSMA-DFO

	Lesions interpreted as PSMA-positive with 89Zr-PSMA-DFO in PET-2						
Patient	PET finding	Ratio SUV_{max}: MBP_{mean}, day 1	Ratio SUV_{max}: MBP_{mean}, day 2	Ratio SUV_{max}: MBP_{mean}, day 3	Ratio SUV_{max}: MBP_{mean}, day 6	Corresponding area with ^{18}F-JK-PSMA-7 in PET-1, ratio SUV_{max}:MBP_{mean} (2 h)	Corresponding area with ^{68}Ga-PSMA-11 in PET-1, ratio SUV_{max}:MBP_{mean} (1 h)
1	Prostate lobe right		13.5	10.1		4.6	
	Prostate lobe left		9.7	5.5		4.0	
2	Lung left (dignity unclear)		7.6		13.3		3.3
3	l.n. retroperitoneal		4.8	11.3		0.8	
	l.n. retroperitoneal		26.2	20.4		1.3	
	l.n. retroperitoneal		21.9	16.5		0.9	
	l.n. supraclav. left		18.6	12.7		1.2	
6	l.n. iliac right		10.5	19.9			0.9
	Os ilium left		19.4	23.9			1.7
8	l.n. retroperitoneal	8.5	9.9		21.7		1.8
	l.n. retroperitoneal	9.1	8.6		10.0		3.5
	l.n. supraclav. left	2.4	2.5		11.3		1.2
10	Prostate fossa right		11.9	17.8	NA	6.7	
13	l.n. iliac right		19.6	11.5			6.1
14	Prostate fossa left		28.1	12.0		8.4	

When one or several PSMA-positive areas were detected by ^{89}Zr-PSMA-DFO PET, the SUV_{max} within the corresponding area of the ^{18}F-JK-PSMA-7 or the ^{68}Ga-PSMA-11 PET was measured. The SUV_{max} within the suspicious area was divided by the SUV_{mean} in the mediastinal blood pool. The ratio SUV_{max} (lesion): SUV_{mean} (MBP) was a measure of the contrast between the suspicious area and the background. The ratio of the ^{89}Zr-PSMA-DFO PET-2 (first measurement) was significantly higher than the ratio of the PET-1 scan with ^{68}Ga-PSMA-11 or ^{18}F-JK-PSMA-7 in the corresponding areas ($P < 0.0001$, paired t test). In patient 10, the PET scan on day 6 was confined to the pelvis and the ratio between lesion and the MBP was not calculated

l.n. = lymph node; MBP = mediastinal blood pool; NA = not available.

TABLE 5
Image Quality Obtained with ^{89}Zr-PSMA-DFO, ^{18}F-JK-PSMA-7, and ^{68}Ga-PSMA-11 on the Biograph mCT 128 Flow PET/CT scanner

		^{89}Zr-PSMA-DFO PET/CT					
Patient	Parameter (liver)	Day 1	Day 2	Day 3	Day 6	^{18}F-JK-PSMA-7 PET/CT (2 h)	^{68}Ga-PSMA-11 PET/CT (1 h)
1	$SUV_{mean} \pm SD$		2.3 ± 1.2	2.1 ± 1.0		13.1 ± 2.4	
	SNR		1.9	2.0		5.5	
2	$SUV_{mean} \pm SD$		2.7 ± 1.3		2.1 ± 1.4		6.0 ± 1.4
	SNR		2.1		1.5		4.5
3	$SUV_{mean} \pm SD$		2.4 ± 1.8	2.1 ± 1.2		16.3 ± 2.0	
	SNR		1.4	1.8		8.1	
4	$SUV_{mean} \pm SD$	2.9 ± 1.0		1.9 ± 0.8		8.5 ± 1.1	
	SNR	2.8		2.4		8.1	
5	$SUV_{mean} \pm SD$		2.6 ± 1.2	2.6 ± 1.2		13.4 ± 1.8	
	SNR		2.3	2.2		7.6	
6	$SUV_{mean} \pm SD$		2.2 ± 1.4	2.0 ± 0.9			5.0 ± 1.7
	SNR		1.6	2.2			3.0
7	$SUV_{mean} \pm SD$	2.5 ± 1.1	2.3 ± 1.0			10.6 ± 1.7	
	SNR	2.3	2.3			6.4	
8	$SUV_{mean} \pm SD$	3.0 ± 1.1	2.7 ± 0.9		2.3 ± 1.4		4.5 ± 1.0
	SNR	2.6	3.0		1.6		4.5
9	$SUV_{mean} \pm SD$		2.5 ± 1.2	2.5 ± 1.2		10.7 ± 1.4	
	SNR		2.1	2.1		7.8	
10	$SUV_{mean} \pm SD$		2.7 ± 1.3	1.9 ± 0.9		11.9 ± 2.4	
	SNR		2.2	2.2		5.0	
11	$SUV_{mean} \pm SD$		2.8 ± 1.2	2.3 ± 0.9		14.7 ± 1.7	
	SNR		2.4	2.6		8.5	
12	$SUV_{mean} \pm SD$		2.7 ± 1.3	2.5 ± 1.0		14.1 ± 2.2	
	SNR		2.1	2.5		6.4	
13	$SUV_{mean} \pm SD$		1.5 ± 1.3	1.5 ± 0.9			3.5 ± 1.3
	SNR		1.1	1.7			2.8
14	$SUV_{mean} \pm SD$		2.9 ± 1.0	2.4 ± 1.3		14.6 ± 2.9	
	SNR		2.9	1.9		5.1	

The SNR was calculated as the ratio of SUV_{mean} to SD in a VOI with 3 cm diameter in the liver. Image quality was significantly higher with ^{18}F-JK-PSMA-7 ($P < 0.0001$, paired t test) and ^{68}Ga-PSMA-11 ($P = 0.0034$) than with ^{89}Zr-PSMA-DFO.

TABLE 6
CNR of 15 Lesions in 8 Patients with ^{89}Zr-PSMA-DFO PET Scan Results (PET-2) Interpreted as PSMA-Positive

	CNR in the lesions interpreted as PSMA-positive with ^{89}Zr-PSMA-DFO in PET-2						
Patient	PET finding	CNR, day 1	CNR, day 2	CNR, day 3	CNR, day 6	Corresponding area with ^{18}F-JK-PSMA-7 in PET-1, CNR (2 h)	Corresponding area with ^{68}Ga-PSMA-11 in PET-1, CNR (1 h)
1	Prostate lobe right		3.8	3.0		0.9	
	Prostate lobe left		3.5	1.1		0.6	
2	Lung left (dignity unclear)		20.3		23.7		12.1
3	l.n. retroperitoneal		1.1	3.1		0.1	
	l.n. retroperitoneal		8.3	6.6		1.1	
	l.n. retroperitoneal		8.6	4.7		−0.2	
	l.n. supraclav. left		18.8	11.9		2.9	
6	l.n. iliac right		11.5	20.6			3.0
	Os ilium left		17.7	37.9			9.4
8	l.n. retroperitoneal	4.6	4.9		12.2		0.03
	l.n. retroperitoneal	3.9	6.5		5.5		1.7
	l.n. supraclav. left	3.0	3.1		13.0		0.7
10	Prostate fossa right		3.5	13.2	8.4	−0.2	
13	l.n. iliac right		12.9	8.0			4.3
14	Prostate fossa left		30.8	16.7		−0.3	

When one or several PSMA-positive areas were detected by ^{89}Zr-PSMA-DFO PET, the SUV_{mean} within the corresponding area of the ^{18}F-JK-PSMA-7 or the ^{68}Ga-PSMA-11 PET was measured. The CNR was calculated as the ratio of the difference of the SUV_{mean} in the lesion and the SUV_{mean} in the background to SD in the background. The SUV_{mean} of the background and its SD were measured in a 3-cm VOI in the local background around the lesion. The CNR of ^{89}Zr-PSMA-DFO PET-2 (first measurement) was significantly higher than the CNR of the PET-1 scan with ^{68}Ga-PSMA-11 ($P = 0.0016$, paired t test) or ^{18}F-JK-PSMA-7 ($P = 0.036$).

l.n. = lymph node.

However, our logistics for tracer injection and PET scans on different days were designed for a few patients with a rare constellation of inclusion criteria. Very late time points (up to 6 d after tracer injection) might occasionally identify additional lesions but should be combined with earlier image acquisition time points, because PET/CT scans after 6 d exhibit a decrease in the SNR. In the future, the technology of a digital PET/CT will allow lower activities to be applied than those used here with ^{89}Zr-PSMA-DFO (*21*).

Hence, our data provide a solid rationale to further evaluate the performance of ^{89}Zr-PSMA-DFO in prospective clinical trials and overcome potential limitations of our first-in-humans study. Since our study was not designed as a prospective clinical trial, readers were not masked regarding the PSMA PET tracers. Furthermore, the sensitivity of ^{89}Zr-PSMA-DFO cannot be compared in an unbiased manner, because ^{89}Zr-PSMA-DFO PET scans were obtained only in patients with a negative, prior PET scan using ^{68}Ga-PSMA-11 or ^{18}F-JK-PSMA-7. It might have increased the sensitivity of the ^{89}Zr-PSMA-DFO PET that readers could revisit their initial interpretation of the ^{68}Ga-PSMA-11 PET or the ^{18}F-JK-PSMA-7 PET scans based on the ^{89}Zr-PSMA-DFO PET scan in ambiguous cases.

CONCLUSION

^{89}Zr-PSMA-DFO allows more time for ligand internalization and renal clearance before image acquisition, whereas existing PSMA tracers require image acquisition within a few hours of injection. Our findings suggest that ^{89}Zr-PSMA-DFO might be used in men with BCR after a PET/CT scan with established PSMA tracers was read as negative. In particular, acquiring ^{89}Zr-PSMA-DFO PET/CT scans 2 or 3 d after tracer injection might be beneficial in patients with detectable but low PSMA expression in the recurrent tumor lesions, in which the search for PSMA-positive lesions has proven challenging.

DISCLOSURE

Bernd Neumaier and Alexander E. Drzezga have applied for a patent on ^{18}F-JK-PSMA-7. No other potential conflict of interest relevant to this article was reported.

KEY POINTS

QUESTIONS: Does ^{89}Zr-PSMA-DFO exhibit a higher detection rate for subtle tumor lesions than existing PSMA tracers?

PERTINENT FINDINGS: ^{89}Zr-PSMA-DFO detected PSMA-positive lesions in 8 of 14 prostate cancer patients with a negative PET scan acquired previously with existing PSMA PET tracers. Most of the PSMA-positive patients had oligometastatic status or a local relapse.

IMPLICATIONS FOR PATIENT CARE: On the basis of the ^{89}Zr-PSMA-DFO PET scan, metastasis-directed radiotherapy was initiated in 5 of 8 patients. ^{89}Zr-PSMA-DFO may therefore offer a benefit to patients with weak PSMA positivity, in whom the localization of recurrent tumor lesions has proved challenging using existing PSMA tracers. Our data suggest that ^{89}Zr-PSMA-DFO might be used in combination with established PSMA tracers, but larger clinical cohorts will be required to characterize and confirm the clinical benefits of ^{89}Zr-PSMA-DFO.

REFERENCES

1. Perera M, Papa N, Roberts M, et al. Gallium-68 prostate-specific membrane antigen positron emission tomography in advanced prostate cancer: updated diagnostic utility, sensitivity, specificity, and distribution of prostate-specific membrane antigen-avid lesions—a systematic review and meta-analysis. *Eur Urol.* 2020;77:403–417.
2. Carlucci G, Ippisch R, Slavik R, et al. ^{68}Ga-PSMA-11 NDA approval: a novel and successful academic partnership. *J Nucl Med.* 2021;62:149–155.
3. Dietlein F, Kobe C, Neubauer S, et al. PSA-stratified performance of ^{18}F- and ^{68}Ga-PSMA PET in patients with biochemical recurrence of prostate cancer. *J Nucl Med.* 2017;58:947–952.
4. Bravaccini S, Puccetti M, Bocchini M, et al. PSMA expression: a potential ally for the pathologist in prostate cancer diagnosis. *Sci Rep.* 2018;8:4254.
5. Ferraro DA, Rüschoff JH, Muehlematter UJ, et al. Immunohistochemical PSMA expression pattern of primary prostate cancer tissue are associated with the detection rate of biochemical recurrence with ^{68}Ga-PSMA-11-PET. *Theranostics.* 2020;10:6082–6094.
6. Muñoz Vázquez S, Endepols H, Fischer T, et al. Translational development of a Zr-89-labeled inhibitor of prostate-specific membrane antigen for PET imaging in prostate cancer. *Mol Imaging Biol.* 2022;24:115–125.
7. Hohberg M, Kobe C, Täger P, et al. Combined early and late [^{68}Ga]PSMA-HBED-CC PET scans improve lesion detectability in biochemical recurrence of prostate cancer with low PSA levels. *Mol Imaging Biol.* 2019;21:558–566.
8. Hohberg M, Kobe C, Krapf P, et al. Biodistribution and radiation dosimetry of [^{18}F]-JK-PSMA-7 as a novel prostate-specific membrane antigen-specific ligand for PET/CT imaging of prostate cancer. *EJNMMI Res.* 2019;9:66.
9. Lee YS, Kim JS, Kim JY, et al. Spatial resolution and image qualities of Zr-89 on Siemens Biograph TruePoint PET/CT. *Cancer Biother Radiopharm.* 2015;30:27–32.
10. Kuhnert G, Boellaard R, Sterzer S, et al. Impact of PET/CT image reconstruction methods and liver uptake normalization strategies on quantitative image analysis. *Eur J Nucl Med Mol Imaging.* 2016;43:249–258.
11. Eiber M, Herrmann K, Calais J, et al. Prostate cancer molecular imaging standardized evaluation (PROMISE): Proposed miTNM classification for the interpretation of PSMA-ligand PET/CT. *J Nucl Med.* 2018;59:469–478.
12. Rowe SP, Pienta KJ, Pomper MG, Gorin MA. Proposal for a structured reporting system for prostate-specific membrane antigen-targeted PET imaging: PSMA-RADS Version 1.0. *J Nucl Med.* 2018;59:479–485.
13. The International Commission on Radiological Protection (ICRP). *ICRP Publication 60: 1990 Recommendations of the International Commission on Radiological Protection. Ann ICRP.* 1991;21(1–3).
14. Dietlein M, Kobe C, Kuhnert G, et al. Comparison of [^{18}F]DCFPyL and [^{68}Ga]Ga-PSMA-HBED-CC for PSMA-PET imaging in patients with relapsed prostate cancer. *Mol Imaging Biol.* 2015;17:575–584.
15. Dietlein F, Hohberg M, Kobe C, et al. An ^{18}F-labeled PSMA ligand for PET/CT of prostate cancer: first-in-humans observational study and clinical experience with ^{18}F-JK-PSMA-7 during the first year of application. *J Nucl Med.* 2020;61:202–209.
16. Dietlein F, Kobe C, Hohberg M, et al. Intraindividual comparison of ^{18}F-PSMA-1007 with renally excreted PSMA ligands for PSMA-PET imaging in patients with relapsed prostate cancer. *J Nucl Med.* 2020;61:729–734.
17. Connor MJ, Smith A, Miah S, et al. Targeting oligometastasis with stereotactic ablative radiation therapy or surgery in metastatic hormone-sensitive prostate cancer: a systematic review of prospective clinical trial. *Eur Urol Oncol.* 2020;3:582–593.
18. Cornford P, van den Bergh RCN, Briers E, et al. EAU-EANM-ESTRO-ESUR-SIOG guidelines on prostate cancer. Part II 2020 update: treatment of relapsing, metastatic, and castration-resistant prostate cancer. *Eur Urol.* 2021;79:263–282.
19. Phillips R, Yue Shi W, Deek M, et al. Outcomes of observation vs stereotactic ablative radiation for oligometastatic prostate cancer: the ORIOLE phase 2 randomized clinical trial. *JAMA Oncol.* 2020;6:650–659.
20. O'Donoghue JA, Danila DC, Pandit-Taskar N, et al. Pharmacokinetics and biodistribution of a [^{89}Zr]Zr-DFO-MSTP2109A anti-STEAP1 antibody in metastatic castration-resistant prostate cancer patients. *Mol Pharm.* 2019;16:3083–3090.
21. Zhang J, Maniawski P, Knopp MV. Performance evaluation of the next generation solid-state digital photon counting PET/CT system. *EJNMMI Res.* 2018;8:97.